SCIENTIFIC PAPER
Published: March 14, 2024
https://doi.org/10.13167/2024.28.3

Comparative probability-based seismic safety assessment of base-isolated buildings: A case study

Peyman Narjabadifam[1], Somayeh Mollaei[1], Ehsan Noroozinejad Farsangi[2], Mehdi Babaei[1] and Navid Mousavi[1]

[1] University of Bonab, Faculty of Engineering, Department of Civil Engineering, Velayat Highway, 5551395133, Bonab, East Azerbaijan, Iran

[2] Western Sydney University, Urban Transformations Research Centre (UTRC), NSW, Australia

Corresponding author:
Ehsan Noroozinejad Farsangi
ehsan.noroozinejad@westernsydney.edu.au

Received:
September 3, 2023

Accepted:
December 8, 2023

Published:
March 14, 2024

Citation:
Narjabadifam, P. et al. Comparative probability-based seismic safety assessment of base-isolated buildings: A case study. *Advances in Civil and Architectural Engineering,* 2024, 15 (28), pp. 33-49. https://doi.org/10.13167/2024.28.3

ADVANCES IN CIVIL AND ARCHITECTURAL ENGINEERING (ISSN 2975-3848)

Faculty of Civil Engineering and Architecture Osijek
Josip Juraj Strossmayer University of Osijek
Vladimira Preloga 3
31000 Osijek
CROATIA

Abstract:
Seismic fragility curves are used to assess the structural vulnerability probability at various damage states. In this study, the effects of different isolation systems on the seismic safety of a two-dimensional reinforced concrete moment-resisting frame are investigated. The reference structure was a hotel building in California, USA. A comparative probability-based seismic safety assessment for building components was conducted on the superstructure hypothetically fitted with various isolation systems. In this regard, two categories of isolation systems, including rubber- and friction-based systems, were selected. The high damping rubber bearings and friction pendulum systems were considered. Incremental dynamic analyses were conducted for a suite of earthquake records to develop the fragility curves considering modelling, demand, and capacity uncertainties. Based on the results, it was observed that the building failure probability reduction was influenced by the seismic isolation systems rather than the fixed base (un-retrofitted) model. Furthermore, the high damping rubber bearings system was found to be more reliable than the friction pendulum system in the limit states considered. However, no significant discrepancy was observed in the performance of the building fitted with isolation systems at higher damage states.

Keywords:
fragility curve; seismic isolation; damage state; incremental dynamic analysis

1 Introduction

Mitigating the irreversible damage from earthquakes has always been the ultimate goal of seismic engineering scholars and scientists. Base isolation systems are one of the best methods to control the seismic performance of structures owing to their plasticity and energy dissipation mechanisms [1]. Owing to their good performance under earthquake loads, isolator systems are widely used in the design of new structures and retrofitting of existing buildings [2-6].

Among the most essential passive seismic control systems, which cause energy dissipation in a structure without any external resources, are base isolation systems, friction dampers, viscous fluid dampers, and tuned mass dampers [6-8]. Currently, there are various types of base isolation systems, such as high damping rubber bearings (HDRB), steel plate rubber bearings, lead rubber bearings (LRB), and friction pendulum systems (FPSs) [1]. Previous studies have compared the behaviour of fixed and isolated structures [9-14].

Probability methods are used to evaluate and control the potential damage levels in existing buildings against seismic loads. These methods consider the existing uncertainties, vulnerabilities, and appropriate rehabilitation strategies [15,16]. Many of these methods use fragility curves to study the probable behaviour of structures. Fragility curves show the probability of increasing damage from a certain level to the seismic parameters [17,18]. These curves illustrate the relationship between the uncertainties in the structural capacity and demand to determine the structural performance level.

Kramer [19], in a pioneering study in this field, investigated the effects of adding an LRB system to a reinforced concrete (RC) frame under the effect of seven earthquake records near and far from the fault using fragility curves. Karim and Yamazaki [9] investigated the effects of adding an isolator to the fragility curve of highway bridges. They presented a hybrid method for plotting the fragility curve [9]. Huang et al. [20] studied the performance of an isolated nuclear power plant building under seismic and explosive loads. Similarly, Huang and Whittaker [21] investigated the performance of a nuclear power plant building using a base isolator. Vatanshenas et al. [22] investigated a multifunctional stadium structure under seismic loads with and without LRB base isolators. Zhang and Hou [23] used a fragility function to investigate the effects of isolation devices on the highway bridge performance under seismic loading. Han et al. [24] plotted fragility curves for an old rigid RC building before and after retrofitting with an LRB base isolator using incremental dynamic analysis (IDA).

Bakhshi and Mostafavi [25] investigated the application of an LRB isolator to RC structures using a fragility curve under seismic loads. Hedayati-Dezfuli and Alam [26] investigated the effects of adding elastomeric isolators to a highway bridge under the effects of 30 earthquake records using fragility curves. Joy and Thampan [27] investigated the application of friction pendulum bearings (FPB) in a hospital building. Mansouri et al. [28] compared the effects of the damping ratio of an LRB isolator on the seismic performance of different buildings. Several other researchers have investigated the fragility curves of base-isolated buildings via seismic risk analysis [29-33]. Ferj and Lopez-Garcia [33] compared the fragility curves of a hospital building with and without base isolators. Recently, Saha and Mishra [34] studied the effects of inter-story isolation systems on the seismic fragility of buildings.

In most of the aforementioned studies, the focus was on deriving the fragility curve for a specific type of base isolation system. In this study, the fragility curves of buildings isolated using different isolation systems were studied and compared. The main objective was to compare the effects of different isolation methods on the failure probability at different levels in a multi-story building. The considered structure was rehabilitated using HDRB and FPS isolators. Uncertainties in the modelling, capacity, and demand were also considered. IDA was performed using SeismoStruct [35] for each seismic intensity parameter level. The fragility curves were constructed for each isolated structure.

2 Methodology

2.1 Seismic isolation systems

The structure studied in this study was the structural frame of the Van Nuys State Building on Van Nuys Blvd. in California [36, 37], as previously discussed by Han et al. [24]. The considered seven-story RC moment-resisting frame was designed in 1965 and built in 1966 with details related to old RC buildings in the US. A three-span frame was investigated with slab thicknesses of 10 in (254 mm) on the second floor, 8,5 in (216 mm) on the third to seventh floors, and 8 in (203 mm) on the roof. Further details are presented in Fig. 1 and in a previous study [24].

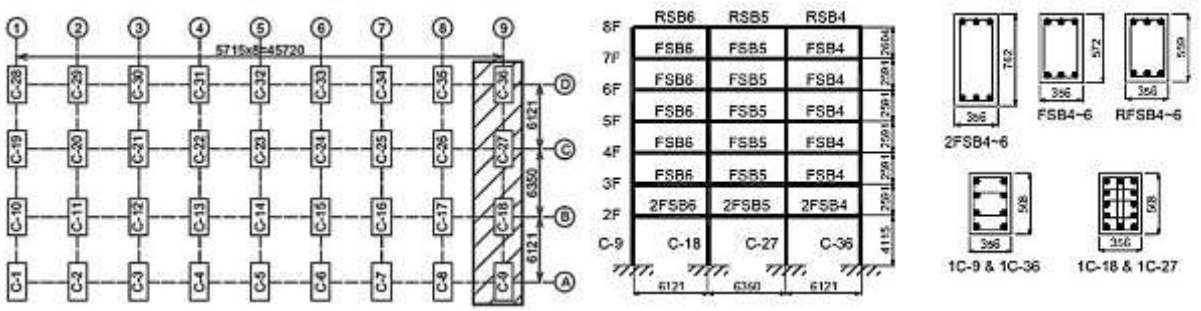

Figure 1. Specification of the reference building frame (without base isolation) considered in this study: a) columns plan; b) elevation; c) cross-sections of the beams and columns

2.2 Design of the seismic isolation systems

As previously mentioned, HDRB and FPS were considered in this study. The main factors in the design of the HDRB isolator are the following: A, the cross-sectional area of the isolator; d, the diameter in a circular isolator; B, the side length in a square isolator; t_r, the thickness of the rubber layer; t_t, the total thickness of the rubber layers; t_s, the thickness of the steel sheets; W, the structural weight and gravitational loading on the isolator (P_{DL+LL}); T_D, the fundamental natural period of the isolated structure; K_{eff}, the effective lateral stiffness of the isolator (which can be calculated using Eq. (1); γ_{eff}, the relative effective shear deformation of rubber ($\gamma \approx$ 100-150); G, the shear modulus of rubber ($G \approx$ 0,40-0,80 MPa at a 100 % shear strain [38]); ξ_{eff}, the effective equivalent damping ratio; D_D, the design displacement (which according to Eq. (2) depends on the seismic intensity of the zone, the spectral coefficient, the fundamental period of structure, and damping of the isolation system); K_1, the initial stiffness ($K_1=K_2/r$); K_2, the post-yielding stiffness ($K_2=GA/t_t$); r, the ratio of initial to post-yielding stiffness (r =1,10-1,15); and Q, the characteristic strength (whose value can be obtained based on the hysteresis curves of the HDRB isolator).

$$K_{eff} = \frac{W}{g} \cdot \frac{2\pi}{T_D}, \qquad (W = P_{DL+LL}) \tag{1}$$

$$D_D = \left[\frac{g}{4\pi^2}\right] \frac{S_{x1} T_D}{B_1} \tag{2}$$

where S_{X1} is the value of the spectral acceleration for T=1 s under the design earthquake and B_1 is a coefficient defined based on the effective equivalent damping ratio.

The main factors in the design of the FPS isolator are the following: RFPS , the radius of curvature of the isolator surface (which can be calculated based on the design period (T_D) using Eq. (3)); μ, the coefficient of friction of the isolator surface; g, the gravitational

acceleration; T_D, the fundamental natural period of the isolated structure; K_1, the initial stiffness (K_1=K_2/r); K_2, the post-yielding stiffness (K_2 = W/R); r, the ratio of initial to post-yielding stiffness (r =1/10-1/15); Q, the characteristic strength (Q = μW); and W, the structural weight and gravitational loading on the isolator (P_{DL+LL}).

$$R_{FPS} = g \times \left(\frac{T_D}{2\pi}\right)^2 \quad (3)$$

According to the design procedure suggested by the Iranian Guidelines for the Design and Practice of Base Isolation Systems in Buildings (Code No.523) [39], the HDRB and FPS isolators for the studied building were calculated as follows in table 1:

Table 1. Calculated HDRB and FPS isolators for the studied building

Types of base isolation systems	Parameters
High Damping Rubber Bearings HDRB	W= 1620 KN (maximum gravitational load from static analysis)
	B_1 = 1,2 (based on the equivalent effective damping)
	S_{x1} = 0,55 g (according to the design spectrum)
	D_D = (9,81/4*π^2)*(0,55*3,7/1,2) = 0,42 m
	K_2 = 0,4 *0,33*1000/0,28 =471,75 kN/m
	K_1 = 471,75/0,1 = 4717,5 kN/m
	F_y = 50,3 kN (from hysteresis curves of the isolator),
	t_t = 0,42/1,5 = 0,28 m
	ξ_{eff} = 10 %
	T_D = 3,7 s
	γ_{eff} = 150 %
	r = 0,1,
	G = 0,4 MPa
	D = 0,65 m
	A = 0,33 m^2
Friction Pendulum System FPS	R_{FPS} = 9,81*(3,7/2π)^2 = 3,4 m
	μ = 2,5 %
	K_2 = 1620/3,4 = 475,73 kN/m
	F_y = 0,025*1620 = 40,5 kN

2.3 Seismic input for IDA

In the IDA method, a significant number of actual earthquake records must be used to logically predict the response of the structure [40]. The acceleration time histories of the earthquake records used in this study are identical to the 32 records used by Han et al. [24]. These records must be scaled to the earthquake spectrum designed by the IDA. All earthquake records were scaled relative to the design spectrum in SeismoMatch [35].

Table 2 lists the specifications of the records used in the study. Based on previous studies [41-43], the spectral acceleration of the first mode with a damping of 5 % Sa (T_1: 5 %) was selected as the earthquake intensity parameter (*IM*). To consider the effects of aftershocks, the results of the main shock and aftershocks are also required in this study. Earthquake records containing multiple aftershocks from the same station as well as earthquake events are rare. Therefore, the MS-AS (Main Shock-After Shock) results used in this study included the main shock and an aftershock recorded back-to-back with a 3-min time interval between the main shock and the aftershock. Han et al. [24] used the results of 32 MS-AS records obtained from CESMD [44] and PEER (NGA) [45].

Table 2. List of earthquake records used

No.	Earthquake	Magnitude	Record name	Station name	Database
1	Coalinga	6,36	NGA_no_368_H-PVY045.AT2	PLEASANT VALLEY P.P. – YARD	PEER NGA
2	Coalinga	6,36	NGA_no_368_H-PVY135.AT2	PLEASANT VALLEY P.P. – YARD	PEER NGA
3	Chalfant Valley	6,19	ChalfantValley86_CE54171P.V2	NO. 54171	CESMD
4	Chalfant Valley	6,19	ChalfantValley86_CE54428P.V2	NO.54428	CESMD
5	Chalfant Valley	6,19	ChalfantValley86_CE54424P.V2	NO.54424	CESMD
6	Imperial Valley	6,53	NGA_no_162_H-CXO315.AT2	CALEXICO FIRE STA	PEER NGA
7	Imperial Valley	6,53	NGA_no_174_H-E11140.AT2	EL CENTRO ARRAY 11	PEER NGA
8	Imperial Valley	6,53	NGA_no_178_H-E03230.AT2	EL CENTRO ARRAY 3	PEER NGA
9	Imperial Valley	6,53	NGA_no_172_H-E01230.AT2	EL CENTRO ARRAY 1	PEER NGA
10	Imperial Valley	6,53	NGA_no_169_H-DLT262.AT2	DELTA	PEER NGA
11	Livermore	5,80	Livermore80A_CE57187P.V2	NO.57187	CESMD
12	Livermore	5,80	Livermore80A_CE67070P.V2	NO. 67070	CESMD
13	Livermore	5,80	NGA_no_212_A-DVD246.AT2	DEL VALLE DAM	PEER NGA
14	Livermore	5,80	NGA_no_214_A-KOD180.AT2	SAN RAMON KODAK BLDG	PEER NGA
15	Livermore	5,80	NGA_no_215_A-SRM070.AT2	SAN RAMON	PEER NGA
16	Livermore	5,80	NGA_no_213_A-FRE075.AT2	FREMONT MISSION S.J.	PEER NGA
17	Livermore	5,80	NGA_no_210_A-A3E236.AT2	HAYWARD CSUH STADIUM	PEER NGA
18	Mammoth Lakes	6,06	NGA_no_231_I-LUL090.AT2	LONG VALLEY DAM UPR L	PEER NGA
19	Mammoth Lakes	6,06	NGA_no_231_I-LUL090.AT2	LONG VALLEY DAM UPR L	PEER NGA
20	Mammoth Lakes	6,06	NGA_no_231_I-LUL090.AT2	LONG VALLEY DAM UPR L	PEER NGA
21	Northridge	6,69	NGA_no_963_ORR090.AT2	CASTAIC - OLD RIDGE ROUTE	PEER NGA
22	Northridge	6,69	NGA_no_1039_MRP090.AT2	MOORPARK	PEER NGA
23	Northridge	6,69	NGA_no_1005_TEM090.AT2	LOS ANGELES - TEMPLE & HOPE	PEER NGA
24	Northridge	6,69	NGA_no_971_ELI180.AT2	ELIZABETH LAKE	PEER NGA
25	Northridge	6,69	NGA_no_945_ANA180.AT2	ANAVERDE VALLEY - CITY RANCH	PEER NGA
26	Northridge	6,69	NGA_no_990_LAC180.AT2	LOS ANGELES - CITY TERRACE	PEER NGA
27	Northridge	6,69	NGA_no_1007_UNI095.AT2	LA-UNIV. HOSPITAL GR	PEER NGA
28	Petrolia	7,20	Petrolia_25Apr1992_CE89530P.V2	NO. 89530	CESMD
29	Petrolia	7,20	Petrolia_25Apr1992_CE89156P.V2	NO. 89156	CESMD
30	Petrolia	7,20	etrolia_25Apr1992_CE89509P.V2	NO. 89509	CESMD
31	Whittier Narrow	5,99	NGA_no_615_A-DWN270.AT2	DOWNEY	PEER NGA
32	Whittier Narrow	5,99	NGA_no_663_A-MTW000.AT2	MT WILSON	PEER NGA

More details regarding the distance from source to site (R), peak ground acceleration (PGA), shear wave velocity in soil (V_s), and Arias intensity characteristics of the earthquake records are listed in Table 3.

Table 3. Characteristics of the earthquake records used in this study

No.	Earthquake	Magnitude	R (km)	PGA (g)	V_s (m/s)	Arias Intensity (m/s)
1	Coalinga	6,36	7,69	0,46	257	4,10
2	Coalinga	6,36	8,41	0,38	257	1,60
3	Chalfant Valley	6,19	14,00	0,24	585	0,20
4	Chalfant Valley	6,19	18,00	0,20	537	0,10
5	Chalfant Valley	6,19	6,00	0,41	316	2,00
6	Imperial Valley	6,53	10,45	0,37	231	0,90
7	Imperial Valley	6,53	12,56	0,68	196	2,00
8	Imperial Valley	6,53	10,70	0,38	163	1,20
9	Imperial Valley	6,53	19,00	0,30	237	0,30
10	Imperial Valley	6,53	22,00	0,39	242	3,30
11	Livermore	5,80	7,00	0,34	550	0,40
12	Livermore	5,80	8,00	0,40	551	0,40
13	Livermore	5,80	23,00	0,27	403	0,20
14	Livermore	5,80	15,00	0,30	377	0,20
15	Livermore	5,80	15,00	0,23	384	0,10
16	Livermore	5,80	34,00	0,31	367	0,00
17	Livermore	5,80	29,00	0,24	517	0,00
18	Mammoth Lakes	6,06	12,00	0,37	537	1,30
19	Mammoth Lakes	6,06	12,00	0,37	537	1,30
20	Mammoth Lakes	6,06	12,00	0,37	537	1,30
21	Northridge	6,69	20,00	0,70	450	3,20
22	Northridge	6,69	16,00	0,36	341	0,90
23	Northridge	6,69	32,00	0,37	332	1,40
24	Northridge	6,69	36,00	0,24	326	0,20
25	Northridge	6,69	37,00	0,15	349	0,10
26	Northridge	6,69	35,00	0,38	365	1,10
27	Northridge	6,69	32,00	0,39	332	1,40
28	Petrolia	7,20	8,00	0,64	250	0,40
29	Petrolia	7,20	8,00	0,66	301	0,45
30	Petrolia	7,20	10,00	0,60	340	1,00
31	Whittier Narrow	5,99	14,00	0,28	271	0,40
32	Whittier Narrow	5,99	14,00	0,29	680	0,30

2.4 Damage index and states

In fragility analysis, the seismic responses of the structure are shown using engineering demand parameters (EDPs). To determine the damage levels of structural components and systems, a capacity model is required that can be described as the damage index (*DI*). DI can be defined as a function of EDPs.

The damage models are often obtained from experimental databanks. The quantitative descriptions of the damage states (*DS*) according to FEMA are presented in Table 4. The superstructure and isolation systems were assumed to be the two main *DS* vulnerable

components of the building. In this study, the *DIs* for the superstructure and isolation systems were considered as the maximum inter-story drift, shear strain for the HDRB, and displacement for the FPS.

Table 4. Capacity values for each building system component

Building component	Damage Index	Limit states				Reference
		Slight	Moderate	Extensive	Collapse	
RC Frame	peak inter story drift ratio (%)	0,50	0,80	2,00	5,99	[24]
HDRB	shear strain (%)	120	160	200	250	[23]
FPS	maximum displacement (mm)	0	50	100	150	[23]

2.5 Finite element modelling

As shown in Figure 2, a two-dimensional (2D) finite element model of the isolated frame was constructed using SeismoStruct [35]. Geometric and material nonlinearities were considered. In the rehabilitated frame, the base isolation system was designed based on ASCE 41 [46], considering the rehabilitation objectives of BSE-1 and BSE-2. These two rehabilitation objectives were equivalent to moderate (MD) and extensive (ED) damage states in HAZUS-MH [47]. The effective seismic mass for each floor was calculated as 1,05*DL* + 0,25*LL* and applied to each beam-to-column joint using a lumped mass element. The dead and live loads were 600 and 200 kg/m^2, respectively.

Figure 2. 2D modelling of the studied frame in SeismoStruct

The material models considered in SeismoStruct for steel and concrete were the stl-mn and conc-ma models, respectively. The Monti-Nutti steel (stl-mn) model is suitable for modelling RC members with the possibility of rebar buckling. The nonlinear concrete (conc-ma) model of Mander et al. [48] was defined based on the Kent–Park material model. The effects of concrete confinement were considered in this model.
In this study, inelastic elements with plastic hinges at both ends were used as the beam and column elements. The plastic hinge length was calculated using Eq. (4) for all elements.

$$L_{pl,cy} = 0{,}2h\left[1 + \frac{1}{3}min\left(9;\frac{L_s}{h}\right)\right] \quad (4)$$

where L_s is the half-length of the element and *h* is the height of the section.
The moment-resisting connections (beam-column joints) were modelled using the method presented by Aboelhassan [49]. The Bil_kin link element is used to define the HDRB isolator.

The first link element is used to model the FPS system. In addition, in the definition of the section fibres in plastic hinges, the compressive strength and ultimate strain of the confined concrete were calculated based on the model proposed by Saatcioglu and Razvi [50].

2.6 Development of the fragility curves

The analytical method for obtaining the fragility curves is based on the analysis of different models under increasing earthquake intensity. By increasing the number of analyses performed, the error decreases, and curves with a higher percentage of confidence are obtained [24]. In this study, an analytical method was used to estimate the fragility curves. A fragility curve is obtained by determining the vulnerability of a structure under certain levels of intensity measure (*IM*). Peak ground displacement (PGD), peak ground velocity (PGV), peak ground acceleration (PGA), first-mode spectral acceleration (Sa (T1)), and spectral intensity can characterise the considered *IM* [41-43]. The fragility function of each structural component for each selected limit state (damage level) can be expressed using Eq. (5), that is, the probability that the seismic demand (*D*) is equal to or greater than the capacity (*C*).

$$P[D \geq C \mid IM] = 1 - \Phi\left[\frac{ln(\hat{C}/\hat{D})}{\sqrt{\beta_{D|IM}^2+\beta_C^2+\beta_M^2}}\right] \quad (5)$$

where Φ is a standard normal distribution function, *IM* represents the magnitude of seismic intensity, $\hat{C}$ is the average value of the structure capacity in a specific damage state, $\check{D}$ is the average value of seismic demand, $\beta_{D|IM}$ and β_C, respectively describe the uncertainty parameters of seismic demand and capacity of the structure, and βM is the parameter describing the modelling uncertainty. The seismic demand parameter is obtained using Eq. (6).

$$EDP = D = a\, IM^b \quad or \quad ln(D) = ln\, a + b\, ln\, IM \quad (6)$$

where *a* and *b* are constant coefficients obtained from the regression analysis of the responses using the IDA method. Additionally, $\beta_{D|IM}$ is obtained using Eq. (7).

$$\beta_{D|IM} = \sqrt{\frac{\sum_{i=1}^{N}\left[ln(EDP_i) - ln\left(a\, IM_i^b\right)\right]^2}{N-2}} \quad (6)$$

where EDP_i is the response (engineering demand parameter) obtained from the IDA for the *i*-th seismic intensity, *N* is the total number of analyses, and aIM_i^b is the demand obtained from the regression analysis for the *i*-th seismic intensity [26].
IDA or dynamic pushover analysis (DPO) is a nonlinear dynamic analysis method that uses scaled earthquake records to determine the *DM* for different *IM* values. Choosing the right *DM* parameter depends on building occupancy, type of structure, and importance [51].
In this study, after performing the incremental dynamic analysis for the isolated structure, fragility curves were drawn for the superstructure in the two isolation cases with HDRB and FPS. The fragility curves of the isolators were also plotted. In this study, modelling and capacity uncertainty values were obtained based on previous studies (β_C and β_M were 0,25 and 0,20; respectively) [52, 53]. Finally, a fragility curve was drawn for each component of the building system.

3 Results and discussion

In Figure 3, the probabilistic seismic demand model (PSDM) obtained here is plotted. A regression analysis was used to determine the ln*D* equations in these graphs. Using this model, the fragility curves were depicted according to the process described in the previous section, and the results are described next.

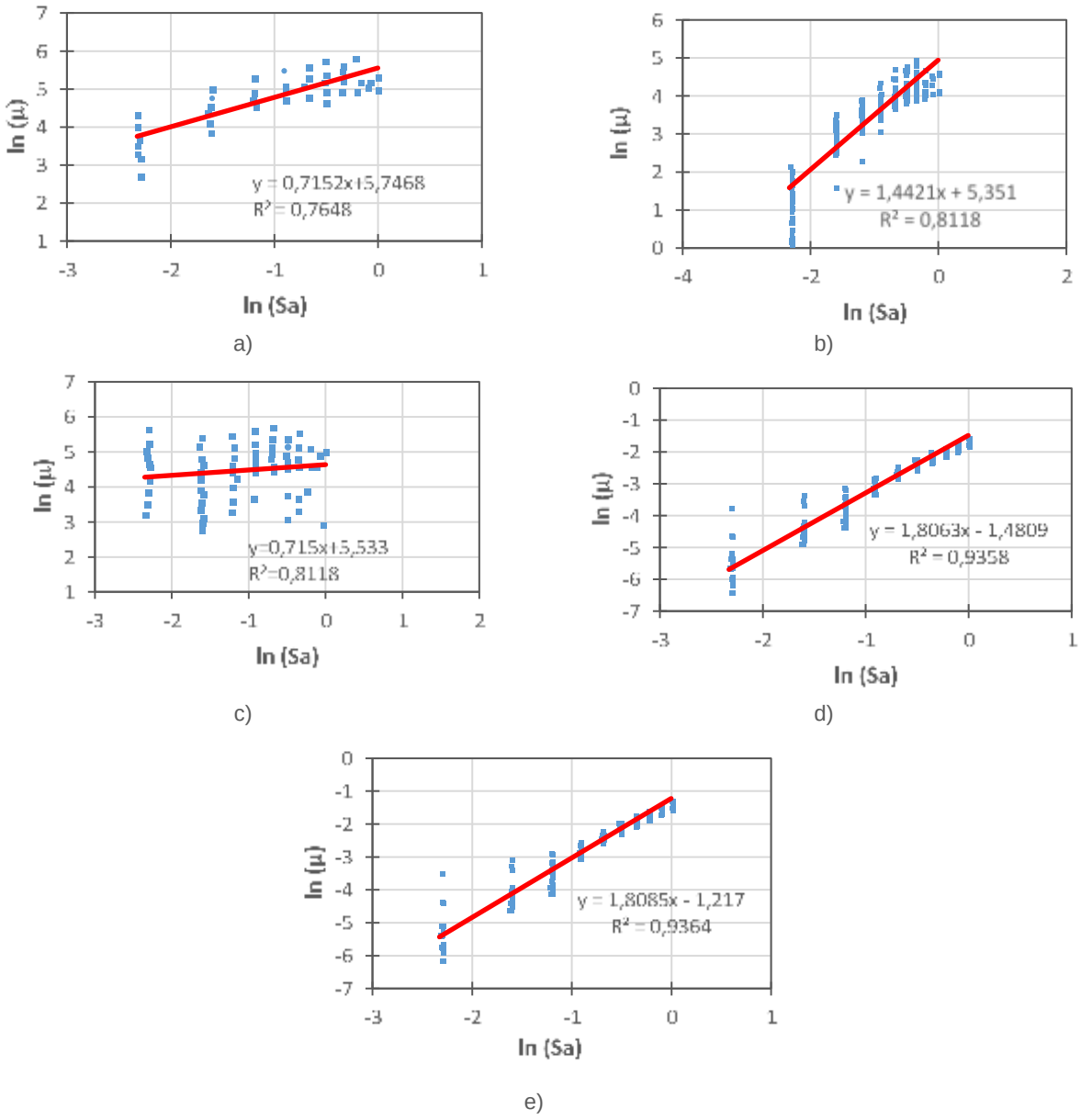

Figure 3. Probabilistic seismic demand model for: a) LRB; b) FPS; c) HDRB; d) superstructure isolated with HDRB; and e) superstructure isolated with FPS

In Figure 4, the fragility curves of the LRB and superstructure isolated with this system are compared with the reference results of [24] to validate the method used in this study. The Sa (T_1) values at BSE-1 and BSE-2 were obtained from uniform hazard spectra constructed based on the USGS hazard map. T_1 is the main period of the non-retrofitted building (T_1 = 1,67 s) and is the median effective period of the building with the isolator (3,70 s) obtained during the design procedure. Although the fragilities of isolated buildings appear to be lower, they cannot be directly compared because of the different fundamental periods. Nonetheless, the annual exceedance probability is lower for S_a (T=3,7 s) than for S_a (T=1,67 s) when the spectral acceleration values are the same. Therefore, the annual exceedance probability was used to directly compare the fragilities of retrofitted and non-retrofitted buildings. The results show good conformity of the fragility curves under the excitation of the main shock and aftershocks

for the isolator and superstructure systems. In addition, as expected, the failure probability of the structure with a fixed base is higher than that of the base-isolated structure.

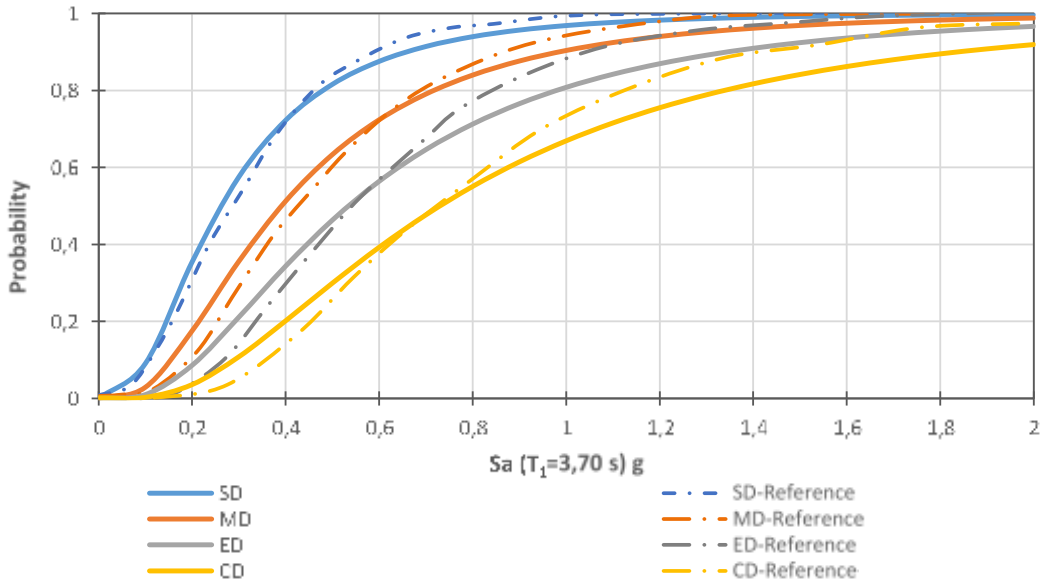

a)

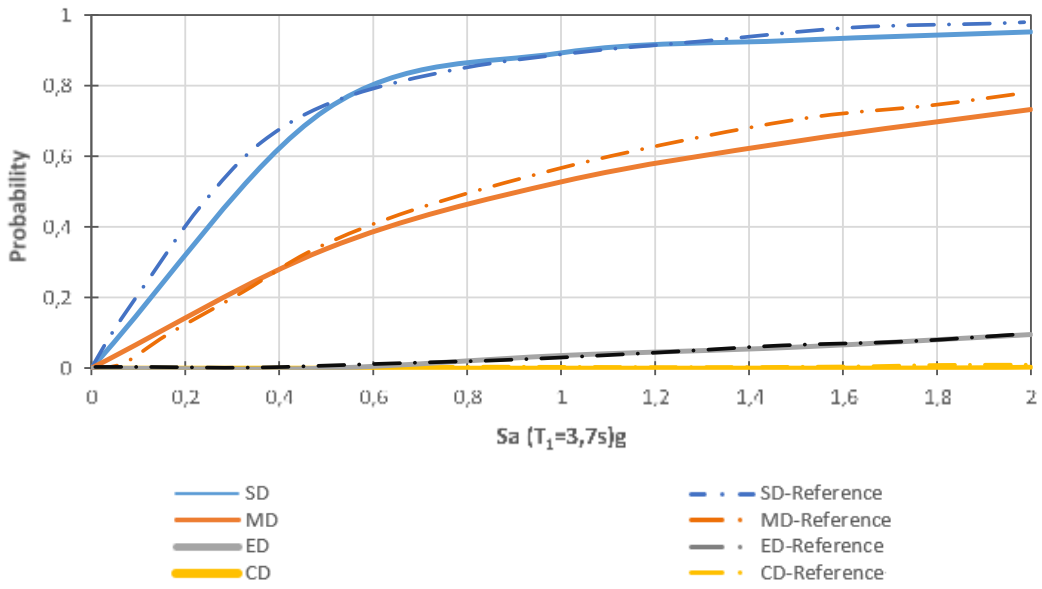

b)

Figure 4. Comparison of the fragility curves in this study with those of the reference model [24] for the: a) LRB; and b) isolated superstructure

In the following section, the fragility curves for the HDRB, FPS, and superstructure in isolated states with both isolators are presented. As shown in Figures 5 a) and b), the probability of fragility of the HDRB is lower than that of the FPS in all damage states. As shown in Figure 5 a), the probability corresponding to the point of S_a (T_1=3,7 s) equal to 0,8 g is 0,05; 0,15; 0,51; and 0,93 at the *CD*, *ED*, *MD*, and *SD* state levels, respectively. The corresponding probabilities at the *CD*, *ED*, *MD*, and *SD* levels are 0,35; 0,57; 0,77; and 0,98; respectively. In addition, the failure probability of the superstructure isolated with the HDRB was lower in the slight and moderate damage (SD and MD) states than that of the superstructure isolated with the FPS. However, in the cases of extensive damage and collapse (*ED* and *CD*), the fragility of the

superstructure with both isolators was almost equal. In other words, the failure probability of an isolated building remains less than 8 % at the extensive and collapse damage levels. By comparing the fragility curves of the fixed-base and isolated structures (Figures 5 c) and d)), it can be concluded that the damage probability of the isolated structure is less than that of the structures with a fixed base, which indicates the effectiveness of the isolator.

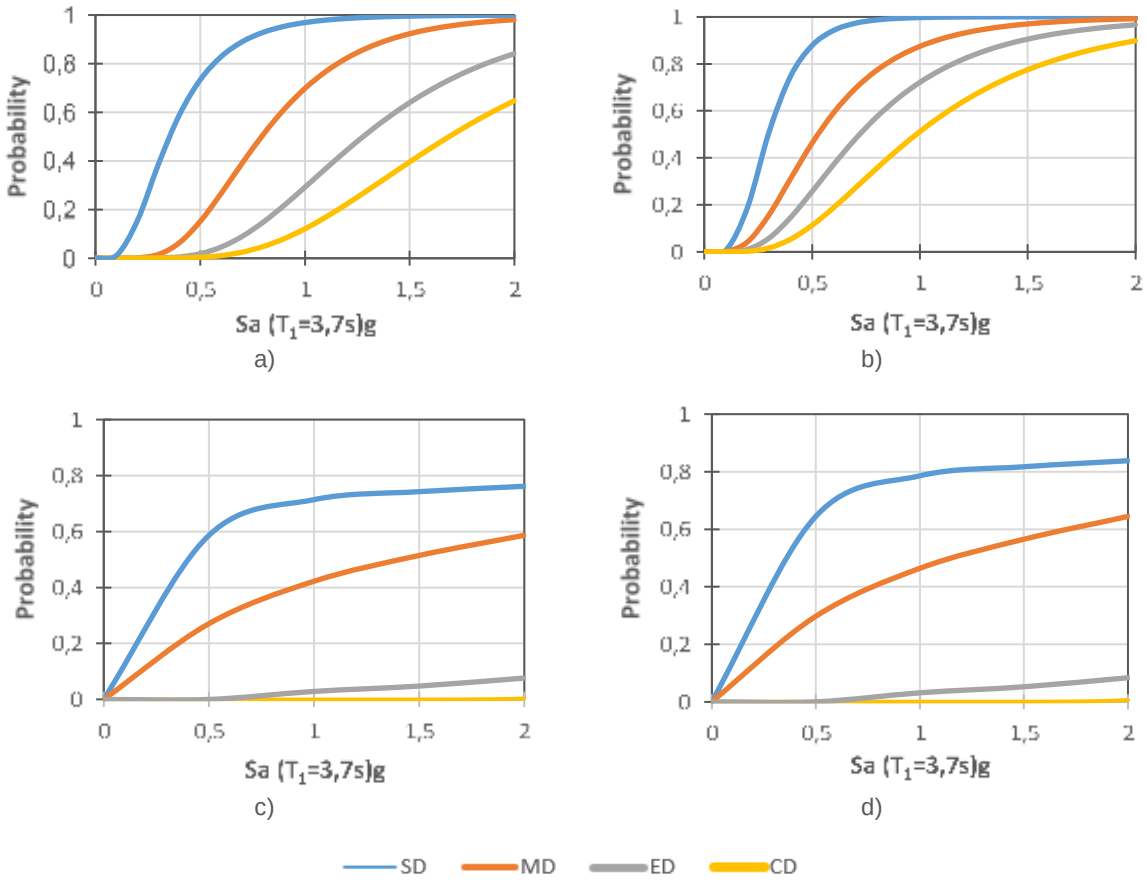

Figure 5. Fragility curves: a) HDRB; b) FPS; c) isolated structure with HDRB; d) isolated structure with FPS

As shown in Figure 6, the probability of failure of the FPS in the slight damage state, when the spectral acceleration of the first mode reaches S_a=1 g, is higher than that of the HDRB. For instance, the failure probabilities are 73 % and 87 % for the HDRB and FPS isolators, respectively, at the Sa (T_1=3,7 s) equal to 0,5 g point. However, with an increase in the acceleration spectrum value, the failure probabilities of the two isolators became similar. In general, the failure probability of the FPS in the moderate and extensive damage states is higher than that of the HDRB. The probability of failure of the FPS in the collapse state is equal to that of the HDRB with an S_a of up to 0,5 g. However, when the value of the spectral acceleration of the first-mode S_a is greater than 0,5 g, the probability of failure of the FPS is greater than that of the HDRB. The failure probabilities of the HDRB and FPS isolators at the *CD* level are 65 % and 84 %, respectively. Overall, the effectiveness of the HDRB isolator is higher than that of the FPS.

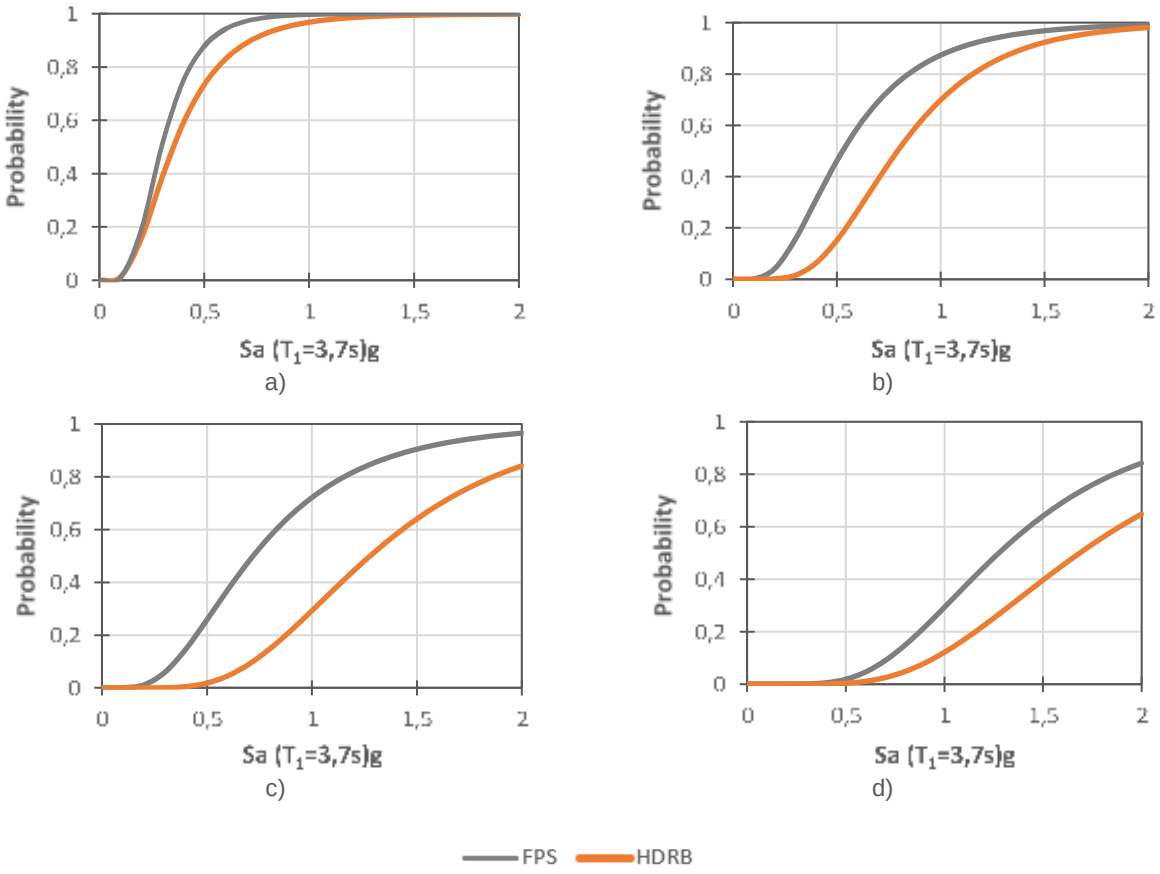

Figure 6. Fragility curves of the HDRB and FPS for damage states: a) slight; b) moderate; c) extensive; d) collapse

As shown in Figure 7, the failure probability of the superstructure isolated with the FPS in a slightly damage state, up to S_a = 0,5 g, is almost equal to that of the superstructure isolated with the HDRB. However, when S_a > 0,5 g, the probability of failure of the superstructure isolated with the FPS is higher than that of the superstructure isolated with the HDRB. In addition, the failure probability of the superstructure isolated with the FPS in the moderate damage state, up to S_a = 0,5 g, is almost equal to that of the superstructure isolated with the HDRB. However, when S_a > 0,5 g, the probability of failure of the superstructure isolated with the FPS is higher than that of the superstructure isolated with the HDRB. However, the failure probability of the LRB-isolated building is higher than those of the two other isolating systems at both the SD and MD levels. The failure probability of the superstructure isolated with the FPS in the extensive damage state, up to S_a = 2 g, is almost equal to that of the superstructure isolated with the HDRB.

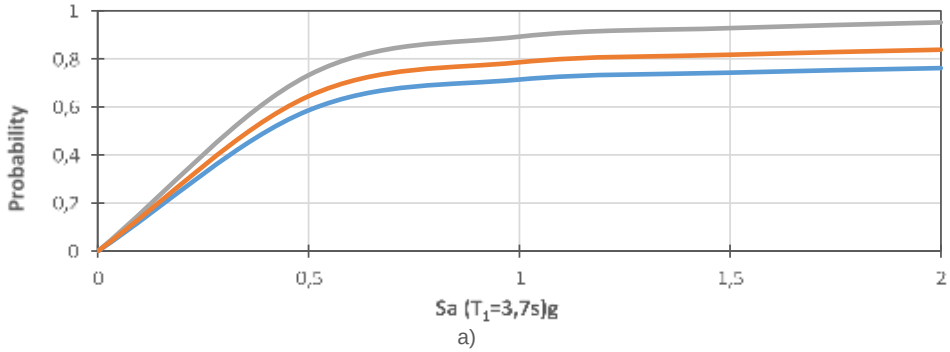

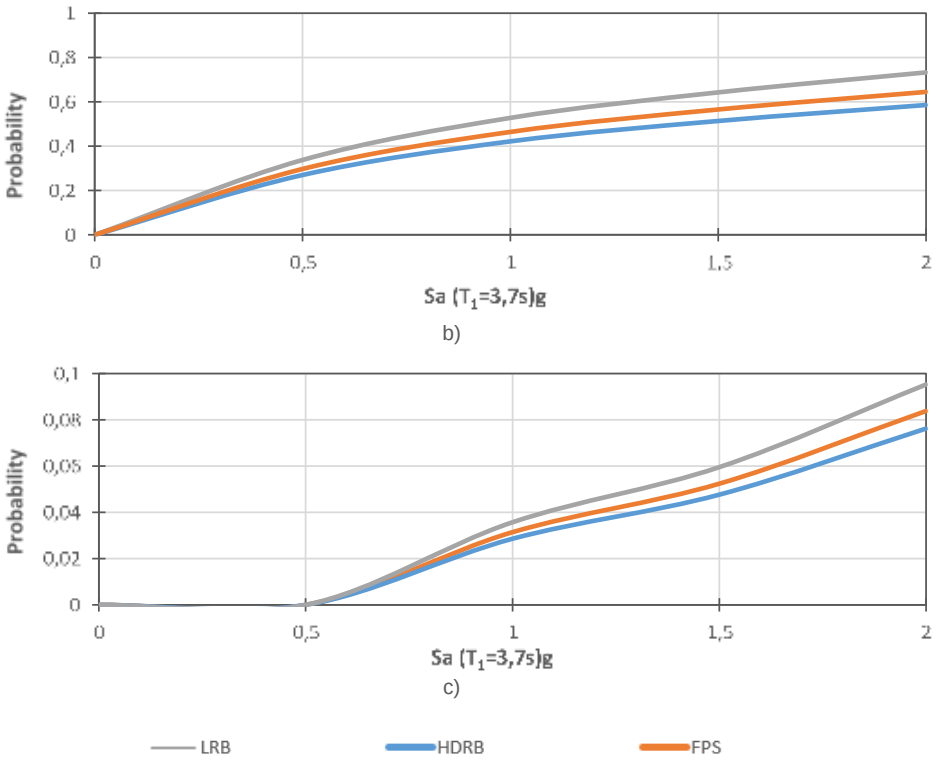

Figure 7. Fragility curves of the superstructure isolated with the HDRB, FPS, and LRB in the damage state: a) slight; b) moderate; c) extensive

By comparing these results with those of the LRB isolator (Figure 7), it can be seen that the failure probabilities of the superstructure isolated with the LRB, HDRB, and FPS in the extensive damage state, up to S_a=2 g, are almost equal. However, the probability of failure of the superstructure isolated with the LRB in the moderate damage state, up to S_a=2 g, is higher than that of the superstructure isolated with the HDRB and FPS systems. In addition, the probability of failure of the superstructure isolated with the LRB isolator in the moderate damage state, up to S_a=2 g, is higher than that of the superstructure isolated with the HDRB and FPS.

4 Conclusions

In this study, the effects of different base isolation systems on the seismic safety of reinforced concrete (RC) building frames were investigated by evaluating their fragility curves. For this purpose, the high damping rubber support (HDRB) system and the friction pendulum system (FPS) were considered. The superstructure considered in this study was a 2D RC moment frame chosen from an existing hotel building in California. Seismic analyses were performed on a set of earthquake records obtained from the Pacific Earthquake Engineering Research Center (PEER) and the Center for Earthquake Seismology Information, which were scaled to the design spectrum of the building. Modelling was performed using SeismoStruct and incremental dynamic analyses were performed. Here, the peak relative displacement of the superstructure stories, the peak shear strain of the HDRB isolator, and the peak horizontal displacement of the FPS were considered as the damage indices. In addition, the spectral acceleration of the first mode (S_a) is regarded as the earthquake intensity parameter. Fragility curves were obtained based on the normal distribution of the statistical average resulting from the linear regression of the damage indices under different earthquake records. Seismic demand, capacity regulation criteria under different damage states, and uncertainties in seismic demand, capacity, and modelling were considered to derive the fragility curves. The main results showed that the failure probability of base-isolated structures, especially at higher

damage levels, was significantly lower than that of non-retrofitted structures. This indicates proper performance of the base isolation system. The influence of the HDRB in reducing the probability of failure was higher than that of the FPS isolator for all damage states. In other words, the failure probability of the superstructure isolated with the HDRB was lower in the slight and moderate damage (*SD* and *MD*) states than that in the superstructure isolated with the FPS. However, in the cases of extensive damage and collapse (*ED* and *CD*), the fragility of the superstructure with both isolators was almost equal. However, the effects of the two types of isolators on reducing the probability of failure at all damage levels were more significant than that of the LRB isolator, which is in agreement with the conclusions of Han et al. [24]. Therefore, HDRB, FPS, and LRB base isolations are suggested as effective systems for seismic risk reduction.

References

[1] Naeim, F.; Kelly, J. M. *Design of Seismic Isolated Structures: From Theory to Practice*. New York: John Wiley & Sons, Inc, 1999. http://dx.doi.org/10.1002/9780470172742

[2] Cardone, D.; Flora, A.; Gesualdi, G. Inelastic response of RC frame buildings with seismic isolation. *Earthquake Engineering & Structural Dynamics*, 2013, 42 (6), pp. 871-889. https://doi.org/10.1002/eqe.2250

[3] Cardone, D.; Gesualdi, G. Seismic rehabilitation of existing reinforced concrete buildings with seismic isolation: a case study. *Earthquake Spectra*, 2014, 30 (4), pp. 1619-1642. http://dx.doi.org/10.1193/110612EQS323M

[4] Cardone, D.; Flora, A. An alternative approach for the seismic rehabilitation of existing RC buildings using seismic isolation. *Earthquake Engineering & Structural Dynamics*, 2016, 45 (1), pp. 91-111. http://dx.doi.org/10.1002/eqe.2618

[5] Mazza, F.; Mazza, M.; Vulcano, A. Nonlinear response of r.c. framed buildings retrofitted by different base-isolation systems under horizontal and vertical components of near-fault earthquakes. *Earthquakes and Structures*, 2017, 12 (1), pp. 135-144. http://dx.doi.org/10.12989/eas.2017.12.1.135

[6] Pal, S.; Roy, B. K.; Choudhury, S. Comparative performance study of tuned liquid column ball damper for excessive liquid displacement on response reduction of structure. *International Journal of Engineering*, 2020, 33 (5), pp. 753-759. https://doi.org/10.5829/ije.2020.33.05b.06

[7] Soong, T. T.; Spencer Jr., B. F. Supplemental energy dissipation: state-of-the-art and state-of-the-practice. *Engineering Structures*, 2002, 24, pp. 243-259. http://dx.doi.org/10.1016/S0141-0296(01)00092-X

[8] Cheng, F. Y.; Jiang, H.; Lou, K. *Smart Structures, Innovative Systems for Seismic Response Control*. 1st Edition, Boca Raton: CRC Press, 2008. http://dx.doi.org/10.1201/9781420008173

[9] Karim, K. R.; Yamazaki, F. Effect of isolation on fragility curves of highway bridges based on simplified approach. *Soil Dynamics and Earthquake Engineering*, 2007, 27 (5), pp. 414-426. http://dx.doi.org/10.1016/j.soildyn.2006.10.006

[10] Sayani, P. J.; Ryan, K. L. Comparative Evaluation of Base-Isolated and Fixed-Base Buildings Using a Comprehensive Response Index. *Journal of Structural Engineering*, 2009, 135 (6), pp. 698-707. http://dx.doi.org/10.1061/(ASCE)0733-9445(2009)135:6(698)

[11] Erduran, E.; Dao, N. D.; Ryan, K. L. Comparative response assessment of minimally compliant low-rise conventional and base-isolated steel frames. *Earthquake Engineering & Structural Dynamics*, 2011, 40 (10), pp. 1123-1141. http://dx.doi.org/10.1002/eqe.1078

[12] Siqueira, G. H.; Sanda, A. S.; Paultre, P.; Padgett, J. E. Fragility curves for isolated bridges in eastern Canada using experimental results. *Engineering Structures*, 2014, 74, pp. 311-324. http://dx.doi.org/10.1016/j.engstruct.2014.04.053

[13] Mohebbi, A.; Ryan, K. L.; Sanders, D. H. Seismic Protection of the Piers of Integral Bridges using Sliding Bearings. *Journal of Earthquake Engineering*, 2017; 21 (8), pp. 1365-1384. http://dx.doi.org/10.1080/13632469.2016.1211567

[14] Jennifer Raj, J.; Vinod Kumar, M. Nonlinear Modal Time History Analysis on RC framed buildings with scrap tyre as the base isolator for Past Indian earthquakes. *Journal of Building Pathology and Rehabilitation*, 2022, 7, 24. https://doi.org/10.1007/s41024-022-00162-5

[15] Porter, K. A.; Beck, J. L.; Shaikhutdinov, R. V. Sensitivity of building loss estimates to major uncertain variables. *Earthquake Spectra*, 2002, 18 (4), pp. 719-743. http://dx.doi.org/10.1193/1.1516201

[16] Yin, Y.-J.; Li, Y. Seismic collapse risk of light-frame wood construction considering aleatoric and epistemic uncertainties. *Structural Safety*, 2010, 32 (4), pp. 250-261. http://dx.doi.org/10.1016/j.strusafe.2010.03.012

[17] Mander, J. B. Fragility curve development for assessing the seismic vulnerability of highway bridges. University at Buffalo, State University of New York, 89, 1999. Accessed: March 11, 2024. Available at: https://citeseerx.ist.psu.edu/document?repid=rep1&type=pdf&doi=02d6253500a128cf1a9daf75172d965e6a43e7d1

[18] Loh, C. H.; Huang, N. J. Seismic fragility analysis of highway bridges (Technical Report). Mid-America Earthquake Center, 2001. Accessed: March 11, 2024. Available at: http://mae.cee.illinois.edu/publications/reports/Report01-06.pdf

[19] Kramer, S. L. *Geotechnical earthquake engineering*. 1st Edition, New Jersey: Prentice-Hall,1996.

[20] Huang, Y. N.; Whittaker, A. S.; Luco, N. Performance Assessment of Conventional and Base-isolated Nuclear Power Plants for Earthquake and Blast Loadings. MCEER-08-0019, 2008. http://dx.doi.org/10.13140/RG.2.1.4371.6727

[21] Huang, Y. N.; Whittaker, A. S. Vulnerability assessment of conventional and base-isolated nuclear power plants to blast loadings. *International Journal of Protective Structures*, 2013, 4 (4), pp. 545-563. http://dx.doi.org/10.1260/2041-4196.4.4.545

[22] Vatanshenas, A.; Sharif Bajestany, D.; Hajihoseinloo, M.; Aghelfard, A. Enhancing the seismic response of a multifunctional stadium equipped with LRB isolators under near-field earthquakes. *Electronic Journal of the Faculty of Civil Engineering Osijek-e-GFOS*, 2018, 9 (17), pp. 11-23. https://doi.org/10.13167/2018.17.2

[23] Zhang, J.; Huo, Y. Evaluating effectiveness and optimum design of isolation devices for highway bridges using the fragility function method. *Engineering Structures*, 2009, 31 (8), pp. 1648-1660. https://dx.doi.org/10.1016/j.engstruct.2009.02.017

[24] Han, R.; Li, Y.; van de Lindt, J. Seismic risk of base isolated non-ductile reinforced concrete buildings considering uncertainties and mainshock–aftershock sequences. *Structural Safety*, 2014, 50, pp. 39-56. http://dx.doi.org/10.1016/j.strusafe.2014.03.010

[25] Bakhshi, A.; Mostafavi, S. A. Development of fragility curves for base isolated RC structures. In: *Proceedings of the 9th International Conference on Structural Dynamics (EURODYN 2014)*, Cunha, Á.; de Sá Caetano, E.; Ribeiro, P.; Müller, G. (eds.). June 30 - July 2 2014, Porto, Portugal, Faculty of Engineering Porto, 2014.

[26] Hedayati Dezfuli, F.; Shahria Alam, M. Effect of different steel-reinforced elastomeric isolators on the seismic fragility of a highway bridge. *Structural Control and Health Monitoring*, 2017, 24 (2), e1866. http://dx.doi.org/10.1002/stc.1866

[27] Joy, R.; Thampan, C. P. V. Seismic Vulnerability Assesment of Tall RC Building with Friction Pendulum System. *International Journal of Civil Engineering*, 2016, 3 (8), pp. 1-8. http://dx.doi.org/10.14445/23488352/IJCE-V3I8P101

[28] Mansouri, I. et al. Seismic fragility estimates of LRB base isolated frames using performance-based design. *Shock and Vibration*, 2017. http://dx.doi.org/10.1155/2017/5184790

[29] Mohamed Nazri, F.; Kian Yern, C.; Moffed Kassem, M.; Noroozinejad Farsangi, E. Assessment of Structure-Specific Fragility Curves for Soft Storey Buildings

Implementing IDA and SPO Approaches. *International Journal of Engineering*, 2018, 31 (12), pp. 2016-2021.

[30] Rezaei Rad, A.; Banazade, M. Probabilistic Risk-Based Performance Evaluation of Seismically Base-Isolated Steel Structures Subjected to Far-Field Earthquakes. *Buildings*, 2018, 8 (9), 128. http://dx.doi.org/10.3390/buildings8090128

[31] Bhandari, M.; Bhart, S. D.; Shrimali, M. K.; Datta, T. K. Seismic Fragility Analysis of Base-Isolated Building Frames Excited by Near- and Far-Field Earthquakes. *Journal of Performance of Constructed Facilities*, 2019, 33 (3). http://dx.doi.org/10.1061/(ASCE)CF.1943-5509.0001298

[32] Gazi, H.; Alhan, C. Reliability of elastomeric-isolated buildings under historical earthquakes with/without forward-directivity effects. *Engineering Structures*, 2019, 195, pp. 490-507. http://dx.doi.org/10.1016/j.engstruct.2019.05.081

[33] Ferj, M.; Lopez-Garcia, D. Comparative Seismic Fragility Analysis of Conventional and Base Isolated Hospital Buildings Having Different Structural Systems. *Journal of Earthquake Engineering*, 2022, 26 (5), pp. 2491-2513. http://dx.doi.org/10.1080/13632469.2020.1767229

[34] Saha, A.; Mishra, S. K. Implications of inter-storey-isolation (ISI) on seismic fragility, loss and resilience of buildings subjected to near fault ground motions. *Bulletin of Earthquake Engineering*, 2022, 20, pp. 899–939. https://doi.org/10.1007/s10518-021-01277-9

[35] Seismosoft, Ltd. Seismosoft 2016, Accessed: March 11, 2024. Available at: https://seismosoft.com/

[36] Pacific Earthquake Engineering Research Center. *Van Nuys hotel building testbed report: exercising seismic performance assessmen*t, Krawinkler, H. (ed.). Berkeley: Pacific Earthquake Engineering Research Center, University of California, 2005. Accessed: March 11, 2024. Available at: https://peer.berkeley.edu/sites/default/files/peer_511_krawinkler_testbed.pdf

[37] Park, S.; Mosalam, K. M. Experimental and analytical studies on reinforced concrete buildings with seismically vulnerable beam-column joints. Berkeley: Pacific Earthquake Engineering Research Center, 2012.

[38] Nishi, T. et al. International investigation of shear displacement capacity of various elastomeric seismic-protection isolators for buildings. *Journal of Rubber Research*, 2019, 22, pp. 33-41. https://doi.org/10.1007/s42464-019-00006-x

[39] Vice Presidency for Strategic Planning and Supervision, Iranian Guideline for Design and Practice of Base Isolation Systems in Buildings- Code No.523, Office of Deputy for Strategic Supervision Bureau of Technical Execution System, Iran, 2010. [In Persian]

[40] Karakaš, N.; Kalman Šipoš, T.; Hadzima-Nyarko, M. Application of different seismic analyses to RC structures. *Journal of the Faculty of Civil Engineering Osijek-e-GFOS*, 2021, 9 (17), pp. 38-51. https://doi.org/10.13167/2018.17.5

[41] Vamvatsikos, D.; Cornell, C. A. Incremental dynamic analysis. *Earthquake Engineering & Structural Dynamics*, 2002, 31 (3), pp. 491-514. https://doi.org/10.1002/eqe.141

[42] Vamvatsikos, D.; Fragiadakis, M. Incremental dynamic analysis for estimating seismic performance sensitivity and uncertainty. *Earthquake Engineering & Structural Dynamics*, 2010, 39 (2), pp. 141-163. http://dx.doi.org/10.1002/eqe.935

[43] Leti, M.; Bilgin, H. Use of Incremental Dynamic Analysis for the seismic performance assessment of RC framed structures. In: *4th International Balkans Conference on Challenges of Civil Engineering, BCCCE*. December 18-19, 2020, Tirana, Albania, EPOKA University; 2020.

[44] Center for Engineering Strong Motion Data. CESMD – A Cooperative Effort. Accessed: March 11, 2024. Available at: http://www.strongmotioncenter.org

[45] Pacific Earthquake Engineering Research Center, PEER, Ground Motion Database. Accessed: March 11, 2024. Available at: http://peer.berkeley.edu/peer_ground_motion_database

[46] American Society of Civil Engineers. ASCE/SEI 41-06*. Seismic rehabilitation of existing buildings*. USA, 2007.
[47] Federal Emergency Management *Agency. Earthquake Model Hazus®-MH 2.1 - Technical Manual*. Accessed: March 11, 2024. Available at: https://www.fema.gov/sites/default/files/2020-09/fema_hazus_earthquake-model_technical-manual_2.1.pdf
[48] Mander, J. B.; Priestley, M. J. N.; Park, R. Observed stress-strain behavior of confined concrete. Journal of Structural Engineering, 1988, 114 (8)- https://ascelibrary.org/doi/abs/10.1061/(ASCE)0733-9445(1988)114:8(1827)
[49] Aboelhassan, M. G. Nonlinear Simulation of Reinforced Concrete Moment Resisting Frames under Earthquakes. *International Journal of Science and Research (IJSR)*, 2021, 10 (3), pp. 736-743. http://dx.doi.org/10.21275/SR21311214003
[50] Saatcioglu, M.; Razvi, S. R. Strength and ductility of confined concrete. *Journal of Structural Engineering*, 1992, 118 (6), pp. 1590-1607. http://dx.doi.org/10.1061/(ASCE)0733-9445(1992)118:6(1590)
[51] Nielson, B. G.; DesRoches, R. Seismic fragility methodology for highway bridges using a component level approach. *Earthquake Engineering & Structural Dynamics*, 2007, 36 (6), pp. 823-839. http://dx.doi.org/10.1002/eqe.655
[52] Padgett, J. E.; Nielson, B. G.; DesRoches, R. Selection of optimal intensity measures in probabilistic seismic demand models of highway bridge portfolios. *Earthquake Engineering & Structural Dynamics*, 2008, 37 (5), pp. 711-725. http://dx.doi.org/10.1002/eqe.782
[53] Celik, O. C.; Ellingwood, B. R. Seismic fragilities for non-ductile reinforced concrete frames–Role of aleatoric and epistemic uncertainties. *Structural Safety*, 2010, 32 (1), pp. 1-12. http://dx.doi.org/10.1016/j.strusafe.2009.04.003